Research Article | Vol. 10, No. 4 | 1 Apr 2019 | BIOMEDICAL OPTICS EXPRESS 2101
Biomedical Optics EXPRESS

Surface cytometer for fluorescent detection and growth monitoring of bacteria over a large field-of-view

RAFAËL SIBILO,[1] JUAN MIGUEL PÉREZ,[1] CEDRIC HURTH,[1,4] AND VALERIO PRUNERI[1,2,3]

[1]*ICFO- Institut de Ciències Fotòniques, The Barcelona Institute of Science and Technology, 08860 Castelldefels, Barcelona, Spain*
[2]*ICREA- Institució Catalana de Recerca i Estudis Avançats, 08010 Barcelona, Spain*
[3]*Valerio.Pruneri@icfo.eu*
[4]*Cedric.Hurth@icfo.eu*

Abstract: Monitoring the early onset of bacterial film formation is critical in many clinical, environmental, and food quality control applications. We built a small inexpensive optical surface cytometer, in contrast with bulk spectroscopic methods, around a light-emitting diode (LED) and a complementary metal-oxide-semiconductor (CMOS) image sensor. It is designed to offer a large field-of-view of 200 mm^2 and a large depth-of-field of 2-3 mm to overcome the limitations of routine methods like spectrophotometry and fluorescence microscopy. It provides a direct measurement without the need for complex image post-processing with a limit-of-detection around 10^4 cells/mm^2, which is competitive with other similar yet more complex devices already available.

1. Introduction

There is a growing need for compact low-cost methods and biosensors, particularly for point-of-care (POC) applications where resources (space, time, and budget) are often very limited. In particular, being able to precisely monitor the presence or the growth of bacterial pathogens is of utmost importance in a large number of clinical and environmental situations as well as for food quality control. Just recently, in July 2018, 13 tourists were hospitalized in Gran Canarias, Spain, for meningitis, blood poisoning, and respiratory diseases, later traced back to infections with Klebsiella pneumonia acquired from hospital visits between January and April. For point-of-care (POC) applications, the monitoring or testing device must be compact, low-cost, and easy to use by minimally trained personnel since it will need to be promptly deployed on the contamination site. In many cases, the growth of biofilms on a surface is a starting point for contamination [1–3]. Indeed, the first step of microbial biofilm formation is the adhesion of a few cells to a surface [1], which is why many state-of-the-art sensors for biofilm detection rely on surface measurements. Multispecies biofilms have shown stronger resistance to antibiotics in a biofilm than when in suspension [3], which is another strong reason to develop accurate methods to measure biofilm formation and take preventive action in the early stages.

The growing need for studying the formation of biofilms is especially directed to the site of possible contamination. Routine monitoring of critical surfaces in a hospital, for instance, often requires an immediate answer so that a rapid decision can be taken before the infection spreads and threatens patients in recovery. This is important since, in the U.S. alone, the Centers for Disease Control (CDC) estimate that hospital-acquired infections (HAIs) account for an estimated 1.7 million infections and 99,000 deaths per year [4]. This means precious time cannot be wasted waiting for the results of an analysis using the often slow and tedious traditional cell culture methods in a dedicated incubator. The answer must be obtained within a few hours, at most. To achieve this requirement, new tools are needed to rapidly treat a

#357986 https://doi.org/10.1364/BOE.10.002101
Journal © 2019 Received 17 Jan 2019; revised 15 Mar 2019; accepted 17 Mar 2019; published 28 Mar 2019

Biomedical Optics EXPRESS

sample from a surface and obtain a count of the bacteria present as soon as possible without the need to ship the swabs to another location.

There are many options available for signal transduction when designing a sensor with a wide range of cost, sensitivity, and specificity. The final choice of a sensor is driven by both scientific and economic considerations and will be determined by the final environment (field or laboratory) where the device will be deployed. Recently, a few elegant approaches with magnetoelastic biosensors that can be directly placed in contact with the food surfaces to be analysed have been proposed [5–7]. The latter is a great advantage because it reduces sample preparation time and enables direct *in situ* measurement but the microfabrication of the sensor is complex and costly whereas the limit-of-detection (LOD) remains rather high. Electrochemical sensors offer the clear advantages of low-cost and easy integration but often require electrode surface modification to provide LOD values relevant to real conditions, namely, i.e. lower than 10^2 cells/mL [8]. Spectroscopic measurements by Raman scattering or Surface-enhanced Raman Scattering (SERS) can lead to multifunctional sensors with high specificity [9] and even direct *in situ* measurements [10]. However, the necessity to fabricate nanostructured surfaces and transport the sample from the examined surface to significantly enhance the detected signal and achieve relevant LOD values as well as the complex signal analysis hinder their widespread development. Quantitative PCR (qPCR) offers the highest sensitivity and specificity but requires efforts for sample collection and preparation [11] due to the facile inhibition of the polymerase reaction by foreign agents that can be present in the samples collected. In addition, qPCR is often time-consuming and requires at least 1 hour to complete enough cycles to amplify the DNA to comfortable signal levels. Considering the variety of fluorescent dyes [12,13] or fluorescent probes [14] available for bacteria detection as well as strong autofluorescence [15], optical methods centered on the detection of fluorescent signals remain the main type of biosensors developed in recent years. The challenge becomes to design and build a low-cost setup while maintaining the high sensitivity enabled by the fluorescent probes and allowing multiplexing [16], especially when the device is meant to be used outside of the laboratory. To reduce the cost and the complexity of the device, colorimetric assays have been developed [17] but the low sensitivity (absorbance) often requires amplification of the bacterial DNA material to reach significant LOD values [17].

Because of the reasons stated above, our aim is to develop a low-cost portable technology. We therefore designed a surface cytometer to measure the fluorescence of bacteria labelled with DNA-intercalating dyes such as SYBR Green I. The reference to a surface is to distinguish this method from bulk spectroscopic methods (turbidity, or fluorimetry). The surface cytometer is designed to be compact using a light-emitting diode (LED) as the light source and a complementary metal-oxide-semiconductor (CMOS) image sensor array (CMOS-ISA) as the detector [18]. Both the LED and a CMOS-ISA were chosen because they are widespread yet sensitive components already available in smartphones, which would make the conversion of our surface cytometer easy to use not only in a laboratory or a clinic but also in low-cost settings, with limited resources, e.g. remote areas in underdeveloped countries. In addition, the main benefit of our approach is to probe a large field of view of about 200 mm^2 thereby decreasing the LOD since a larger area can be analyzed simultaneously. The LOD obtained, about 10^4 cells/mm^2, shows a significant increase from values reported by a similar method concentrating directly on the surface to be probed [8,16]. The device enables real-time growth monitoring because the acquisition time is less than 1 minute per frame. Sample preparation consists in direct sampling and a rapid one-step labelling, which caters to situations where the device must be deployed rapidly at a test site to quantify the non-specific presence of harmful bacterial biofilms. All optical components used are from off-the-shelf suppliers with a few machined parts for added mechanical stability. The overall footprint is small and the weight is kept low for portability and easy deployment. Both the footprint and the weight can still be significantly reduced further by miniaturizing the

Biomedical Optics EXPRESS

optomechanical assembly and the control electronics. We provide a method and supporting data for the reconstruction of bacterial growth curves for internal calibration purposes towards a future application for biofilm monitoring via swabbing and, when needed, using culture or qPCR to amplify the detected material and reach the current LOD.

Shortly after the completion of the present study, closely related work was made available in the literature [19]. In there, Müller at al. describe a similar compact device for bacteria monitoring in contaminated powdered infant formula using fluorescence *in situ* hybridization (FISH) probes. This method provides a specific detection but requires a more complex sample preparation to ensure the FISH probes enter the bacterial cytoplasm. Our approach relies on a non-specific dye that has long been reported to have universal cell permeability [20–22] relatively suitable for assessing the total bacterial count in a sample. It was chosen because it offers a very simple and fast sample preparation technique at the expense of specificity in cases where it is not required.

2. Experimental methods

2.1 Surface cytometer setup

The surface cytometer has a total dimension of 20 cm x 20 cm x 10 cm including the power supply. It is composed of four main modules: an incoherent LED, an optomechanical assembly, a CMOS-ISA, and controlling electronics. Figure 1 shows the schematics of the optics interfacing with the sample slide (Fig. 1(A)) and a photograph of the corresponding so-called surface cytometer (Fig. 1(B)) used in the laboratory.

The light source is a free space high power LED (M470L3, Thorlabs, GmbH), which is band-limited using an interference filter with a center wavelength (CWL) of 466 nm and a bandwidth (BW) of 40 nm (86-352, Edmund Optics Ltd.). The optomechanical assembly comprises optical elements mounted on precision holders creating a vertical optical axis to excite the surface with the light source, collect the emission from the sample, and transmit the optical signal emitted to the CMOS-ISA. The optical elements are assembled as follows. They include: an achromatic doublet lens (Thorlabs AC254-050-A) with an antireflective coating in the 400-700 nm region and an estimated focal length of 49.6 mm at 470 nm, an interference filter with a CWL of 526 nm and a BW of 53 nm (87-241, Edmund Optics Ltd.), a green color filter (46-053, Edmund Optics Ltd.), and an imaging lens with an effective focal length of 6 mm equipped with a manual focus and an iris (Navitar). The achromatic lens was used to confine the light source onto the target surface (sample). All lenses were used in their specified normal working conditions at room temperature, with incident powers below the damage threshold, and limited to the central region of the optical aperture by using diaphragms. Therefore, we do not expect any non-linear behavior nor excessive aberrations. The combination of the interference and color filter allowed for the proper suppression of the excitation wavelength (light source). Even with a high power, non-collimated beam, this combination of filters allowed us to remove the excitation light hitting the surface of the filters at all angles, which improved the signal-to-noise-ratio (SNR) despite a peak transmission coefficient of 70% for the color filter. Using a photodiode sensor (Thorlabs S120C) at 470 nm, we measured a power of 135.2 mW over 94 mm^2 at 470 nm after the excitation filter and 0.750 mW over 1.13 mm^2 at the sample plane. This corresponds to irradiances of 1.44 mW/mm^2 and 0.66 mW/mm^2, respectively. The loss originates from the low collimation of the divergent LED beam, but is still sufficient to obtain the sensitivity needed.

Biomedical Optics EXPRESS

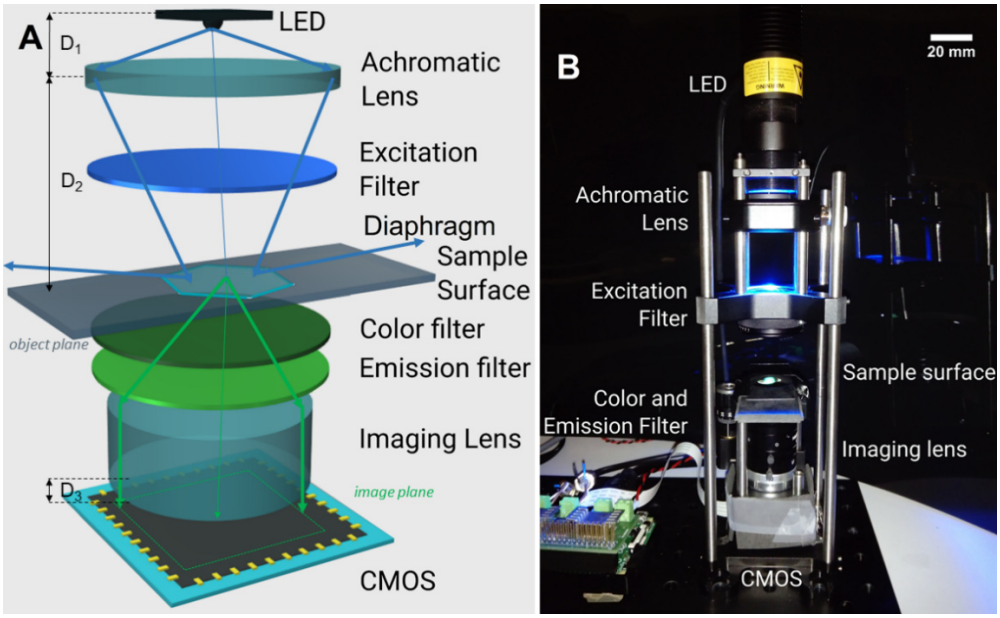

Fig. 1. (A) Details of the optical elements interfacing with the sample. The critical distances were: D_1 = 10 mm between the LED and the achromatic lens, D_2 = 50 mm between the lens and the object, and D_3 = 11 mm between the imaging lens backplane and the CMOS image sensor array (CMOS-ISA). The blue and green arrows represent the limit (bold) and central rays (light) of the excitation and emission paths, respectively. (B) Surface cytometer optical setup including the light-emitting diode (LED) light source, imaging lens, color and interference filters, and the CMOS-ISA. The scaler bar of 20 mm was added for scaling.

2.2 Determination of the field-of-view

The CMOS-ISA is a 4.6-mm diagonal sensor with 3280 x 2464 pixels (Sony IMX219), also known as the version 2 of the Raspberry Pi camera module. We have removed the lens originally mounted over the sensor and restricted the measurements to the central area (2592 x 1944 pixels) to avoid edge effects. We used a positive 1951 USAF test target (R3L1S4P, Thorlabs, GmbH) for the quantification of FOV and spatial resolution. The imaging lens was used to focus the detection on the surface plane and was arranged to obtain a field-of-view of 200 mm^2. According to Fig. 2(B), our system resolves down to Element 5 of Group 4, which corresponds to a resolution of 25.4 lines/mm, or a spatial resolution of 39 µm. Since the objective of the sensor is to detect and process aggregate information of the surface, we increased the FOV while sacrificing spatial resolution. The resulting normalized images of the test target are shown in Fig. 2.

Biomedical Optics EXPRESS

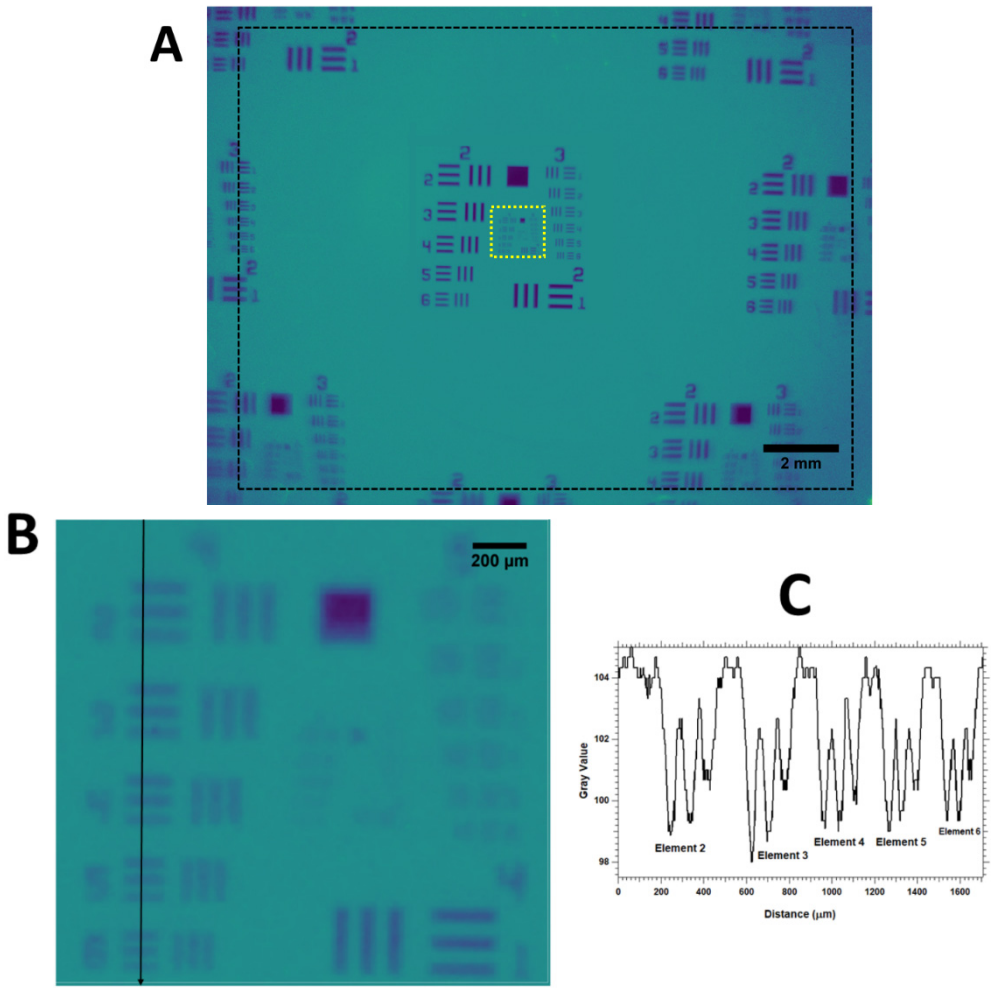

Fig. 2. Determination of the filed-of-view (FOV) and lateral resolution of the device using the positive 1951 USAF target. Entire restricted 200 mm^2 imaging FOV on the CMOS-ISA (A). The dashed yellow square represents Groups 4 and 5 on the calibration grid while the black dashed square delimits the FOV used (16.5 x 12.4 mm). Magnification of Groups 4 and 5 (B) showing the highest resolved elements in Group 4 used to determine the lateral resolution of 25.4 lines/mm (39 µm). Cross-section (C) indicated by the black arrow after conversion in a 16-bit grayscale image.

2.3 Control electronics

The controlling electronics is based on a Raspberry Pi 3 Model B, which processed the electronic signal acquired after detection with the image sensor to provide a fluorescence count proportional to the sample emission level. In order to control the camera using Python, a third party module (picamera) was used. Like most CMOS sensors, the IMX219 uses a Bayer filter configuration to structure its pixels. Every 2 x 2 neighboring pixels contain one red, one blue, and two green pixels. A single capture consists of four two-dimensional arrays with a size of 1640 x 1232 pixels with 10 bits for each pixel. The exposure time and gain of the sensor can also be adjusted using the picamera module. The optimal values were an exposure of 100 ms for a nominal gain of 1.0 at a capture rate of 30 frames/s. An initial 2 s were allowed for gain stabilization before acquiring the image. From the raw data, we developed our own software (Python 2.7.6) to retrieve only the signal corresponding to the

Biomedical Optics EXPRESS

channels of interest (both green channels for the configuration disclosed) and process it to obtain a single fluorescent count proportional to the number of bacteria present on the 200 mm^2 surface. The Raspberry Pi also includes general-purpose input/outputs (GPIOs) to connect miscellaneous electronics. We designed a printed circuit board (PCB) to control the LED. A nominal current of 1A and a forward voltage drop of 3.5V drive the incoherent light source described. A power supply of 5V at 5A feeds the complete system. The LED is therefore operated in a pulsed mode at a duty cycle of 50% and a frequency of 20 MHz (frequency of the pulse-width modulation (PWM) control signal). A quiet time of 2 seconds was used at the beginning of each measurement to stabilize the LED output before acquiring fluorescence data. In addition, the LED was placed on a large Al heat sink, as specified by the manufacturer. In these conditions, we measured a negligible drift of 0.26% of the output power over 17 min (See Appendix, Fig. 6).

2.4 Bacterial growth and incubation

To prepare the analyzed samples and model a situation of rapid proliferation of an opportunistic pathogen, *Escherichia coli* (Invitrogen DH5 alpha strain) was grown at 37°C in LB Broth medium (Scharlau 02-384-500) with an incubator shaker (Thermo Fisher Scientific MaxQ8000). We controlled the bacterial growth by monitoring the optical density (OD) with a spectrophotometer (Thermo Fisher Scientific Nanodrop 2000c) by measuring the optical density at 600 nm (turbidity). We monitored the bacterial growth over the course of 8 hours. For each analyzed time point, an aliquot of the culture was stained and deposited directly on the reader sensor without further processing. Each aliquot was processed in triplicates and 3 acquisitions were averaged for each measurement.

2.5 Bacterial nucleic acid staining

We first confirmed we had enough sensitivity to measure fluorescently-labelled bacteria by measuring serial dilutions of a common dye, namely Alexa Fluor 488 succinimidyl ester (A20000, ThermoFisher Scientific) in deionized water. We determined an approximate LOD of 1-2 nM for the distinction of the fluorescence signal above the system baseline (See Appendix, Fig. 7). In order to monitor bacterial growth with the surface cytometer, *E. coli* cells were labelled with a fluorescent nucleic acid stain, namely SYBR Green 1 (SG), from a 10,000X concentrate stock solution (Invitrogen S7563) in dimethyl sulfoxide (DMSO). SG has a peak absorption at 490 nm and a peak emission at 520 nm. SG intercalates within double-stranded DNA helices without specificity. When it is bound to DNA, the fluorescence is increased by several orders of magnitude. 10 µL of SG stock solution was dissolved into 100 µL of phosphate buffered saline (PBS, Sigma-Aldrich P4417). Each 1 mL of sample was treated with 1 µL of SG. Before each measurement, the samples were incubated for 20 minutes at room temperature. For the purposes of growth monitoring, we labelled and measured samples at different OD values, and compared the surface cytometry results to those obtained with the spectrophotometer and a fluorescence microscope (Nikon Ti inverted microscope with Andor iXon camera). Since the samples were imaged within 20 minutes after taking the culture aliquot, we assumed that a vast majority of bacteria in the sample were alive, as confirmed by using combined staining with propidium iodide (See Appendix, Fig. 8).

2.6 Surface measurement

For the measurements with the surface cytometer, we prepared the surfaces by combining borosilicate cover slips with a 100 µm thickness (Knittel Glass) with silicone isolators (Grace Bio-labs GBL665301) to confine the sample to an area larger than the instrument FOV. Since our interest was in the cells on the surface, signal processing was limited to obtain a mean fluorescence count from the sample. It was correlated to a concentration of bacteria in cells/mm^2 or used to build a complete growth curve similarly to the measurements with the

Biomedical Optics EXPRESS

spectrophotometer. For characterization and comparison purposes, we also imaged the samples with a fluorescence microscope.

3. Results and discussion

The main drive of the present study was to compare the generation of a growth curve using our low-cost platform to standard accepted methods such as absorbance (turbidity) measurements and fluorescence microscopy.

3.1 Reference growth curve using absorbance measurements

One of the most standard methods to measure bacterial growth is using absorbance measurements. Figure 3 shows the average growth curve obtained by averaging the curves measured over several experiments carried out over several weeks growing *Escherichia coli* in liquid LB at 37 °C and collecting an aliquot (50 µL) at the indicated times to perform the absorbance measurement. The data is reported in terms of changes in the optical density (OD), which takes into account various phenomena including scattering and absorption that modify the intensity of the light transmitted by a medium with respect to the incident light flux. Bacterial growth parameters such as the lag time, T_{lag}, or the recovery time to reach a significant cell-division rate after being transferred to a new environment, and the absolute growth rate, k_Z, were determined by fitting the data to the Gompertz-Zwietering model [22,23]:

$$OD(t) = B_G + A_G \exp\left(-\exp\left(\frac{ek_z}{A}\left(T_{lag} - t\right) + 1\right)\right) \quad (1)$$

A_G and B_G are constants used to normalize the experimental data.

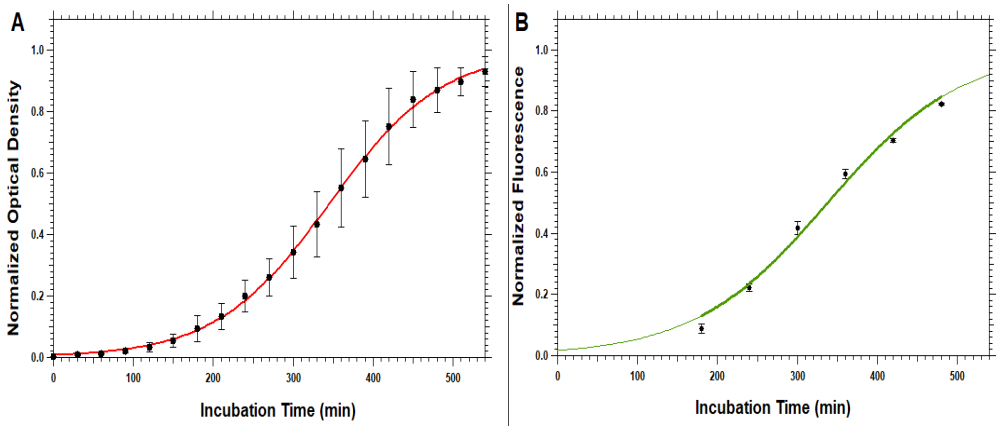

Fig. 3. Average growth curve in liquid phase obtained using optical density measurement, or turbidity, at 600 nm (A). The error bars obtained originate from experiments performed on different days with cells in different dormant states prior to seeding the LB culture medium. The red line is a fit to a logistic population growth model yielding a seed ratio of the inoculum size to the carrying capacity x0 = 0.0077 ± 0.001 and a maximum growth rate r = 0.0140 ± 0.0004 s^{-1}. The growth curve generated by the surface cytometer (B) is in close agreement with the reference optical density curve and yields x0 = 0.017 ± 0.005 and r = 0.0120 ± 0.0009 s^{-1}.

The maximum growth rate, r, and the seed ratio, x_0, of the inoculum size to the maximum carrying capacity were obtained using the logistic population growth model, a subcase of the Richards model well-adapted to bacterial growth [23,24]:

Biomedical Optics EXPRESS

$$OD(t) = B_R + \frac{A_R}{\left(1+\left(\frac{1}{x_0}-1\right)exp(-rt)\right)} \quad (2)$$

A_R and B_R are a different set of constants used to normalize the experimental data.

Figure 3(A) shows the normalized variation of the evolution of the optical density of the 50 µL droplet aliquot at 600 nm and the corresponding fit to the logistic model yielding x_0 = 0.0077 ± 0.001 and r = 0.0140 ± 0.0004 s^{-1}. The curve shows a short lag phase (T_{lag} = 191 ± 14 min), an exponential growth phase from 200 to 450 min and a stationary phase after 500 min. From the Gompertz-Zwietering, k_Z = 0.0035 ± 0.0004 s^{-1}. The data fits particularly well to both models (solid red line in Fig. 2(A) for the logistic growth model) with a residual error χ^2 = 1.67 10^{-3} for the Gompertz-Zwietering model and χ^2 = 1.60 10^{-3} for the logistic growth model, respectively. We can therefore use this growth curve and its parametrization as a reference throughout the present study.

3.2 Growth monitoring using fluorescence microscopy

Another common way to count bacterial cells to determine growth, in particular for biofilm formation studies [1–3], is to apply particle analysis methods to microscopy images recorded either directly in brightfield, in phase-contrast, or in fluorescence using either bacterial autofluorescence [15] or external dyes. SYBR Green is a well-known DNA-intercalating dye with enhanced fluorescence yield when stacked between DNA base pairs [25]. It is by no means a specific marker of bacteria, but we determined it had an irreversible high staining efficiency (> 95%) of bacterial cells with a high signal-to-noise fluorescent signal when excited around 480 nm. In addition, it only requires less than 20 min to stain a 1 mL sample and the low background signal from unbound SYBR Green molecules allows measurement without additional washing steps. To generate the growth curve, a culture aliquot was taken at set times from the initial seeding of the LB medium, stained with SYBR Green by gentle mixing for 15-20 min, then deposited on a glass surface and imaged using fluorescence microscopy. Figure 3(A) shows six of these images representing the fluorescence image at 0, 60, 116, 171, 235, and 292 min of the liquid culture, respectively. The images are background-subtracted using a rolling ball method with a radius of 10 pixels in order to remove autofluorescence from the glass slide as well as contributions from unbound dye and cells outside of the focal plane. Visually, there is a clear increase in the number of bacteria present on the surface and the overall fluorescent intensity. The next step consisted of quantifying this evolution. The images generated were therefore further processed to perform an accurate counting of the number of bacteria present in the microscope field of view (82 x 82 µm) using the particle analysis algorithms of ImageJ. All images were first thresholded using the same settings to restrict the images acquired to the fluorescence signal with an intensity above 29,000 on the 16-bit scale and thus generate a binary image. When a high number of cells are present, it becomes difficult to delimit individual bacteria. We therefore used a watershed algorithm [26] to better separate adjacent bacterial cells and therefore improve the accuracy of the particle counting analysis. In order to accurately select bacterial cells and avoid counting other objects such as debris and surface artefacts, the known typical dimensions of *E. coli* [27,28] to define a minimum acceptable particle area and circularity. Typically, we selected particles above 3 μm^2 with circularity values between 0.0 and 0.8. The circularity c is a parameter that describes how close an object is to a true circle and is defined by [29]:

$$c = 4\pi\frac{A}{P^2} \quad (3)$$

Biomedical Optics EXPRESS

Where A is the area and P the perimeter. A value of 1 indicates a perfect circle whereas c draws closer to 0 for more and more elongated polygonal objects.

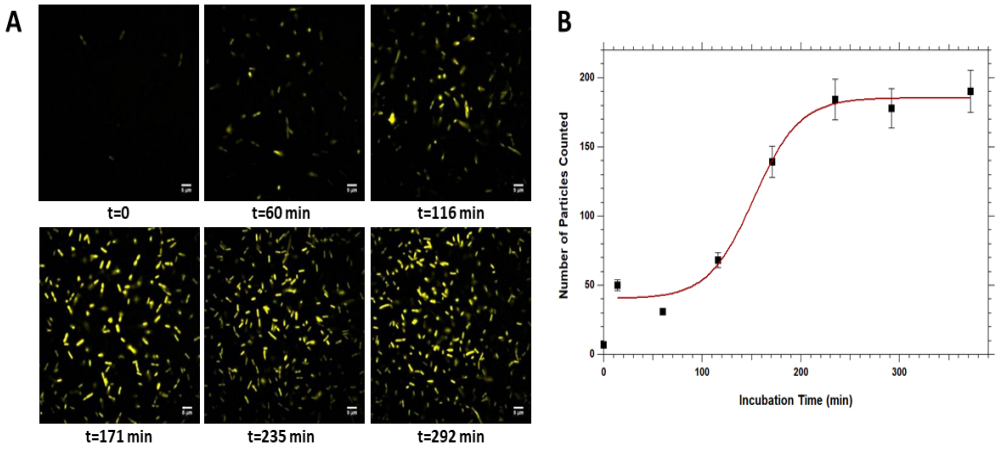

Fig. 4. (A) Time evolution from microscopy images acquired on a Nikon Ti-U microscope to benchmark our device using SYBR Green stained aliquots of *E. coli* growing at 37 °C. The intensity scale is identical for all images and the images have been background subtracted using a rolling ball method with a radius of 10 pixels. (B) Growth curve obtained by particle analysis using a watershed algorithm to better separate adjacent cells, then restricting to a size and circularity according to the expected dimensions of *E. coli* organisms. The red line is a sigmoid fit that represents the expected curve.

Figure 4(B) shows the result of the image processing and the quantification of the recorded frames including those in Fig. 3(A). Each bacteria present in the microscope FOV is counted as a particle given the restricted values accepted for size and circularity. The reconstructed growth curve shows a very short lag phase, similarly to the one obtained by absorbance measurements (Fig. 2(A)), but reaches the stationary phase much earlier and much faster than the reference curve of Fig. 3(A). Compared to Fig. 3(A), the exponential growth phase is much shorter. There are many possible factors contributing to this observation. First, the surface can have an effect on surface growth. Indeed, attachment to a surface can enhance the growth or even promote the assembly of bacteria already grown [30]. However, depositing an aliquot of the culture liquid and imaging it immediately after a short staining period should minimize this effect. Therefore, we believe that the observed shorter exponential growth phase is more likely to be an artefact introduced by the surface, the measurement method and the image processing. Indeed, it is well know that non-fixed cells do not readily adsorb onto a solid surface [31], which is a requirement for a surface-oriented method like microscopy. Furthermore, the imaging method is not able to consider bacteria that are out of the focal plane since the fluorescent signal is too weak and to diffuse to contribute to the image. These two elements can contribute to a significant underestimation of the number of bacteria present in the culture aliquot compared to the bulk measurement performed in the spectrophotometer (Fig. 3(A)). In addition, the particle counting algorithm and the selection parameters we applied are not perfect and can lead to errors in estimating the number of bacteria present, especially at higher concentration when the number of surface sites available to bacteria decreases and more than a monolayer is formed. The analysis of histograms obtained from each image as well as the intensity distribution along a radius of 500 pixels from the center of the image and over 180° (radial profile distribution) could not provide a growth curve comparable to the expected result of Fig. 3(A). This underlines the severe limitations of microscopy techniques towards the study and quantification of bacterial growth. Our proposed direct measurement method can circumvent some of these limitations.

Biomedical Optics EXPRESS

3.3 Growth curve obtained using the surface cytometer

Similarly to the fluorescence microscopy, a culture aliquot was stained with SYBR Green and deposited on the sensing surface of the reader. The background data is acquired with the same camera exposure both when the LED is off and on. The value when the LED is on is then subtracted from the signal shown in Fig. 3(B). To account for the non-uniform camera response, we only consider the signal from the green sub-pixels. Typically, the signal reported is from the green sub-pixels minus the average value of the blue and red sub-pixels to further correct for stray light in the system. The actual CMOS-ISA images (See Appendix, Fig. 9) are generally not stored since we consider the mean signal in the green channel. The field-of-view is much larger than in the microscope, which allows a better averaging of the fluorescent signal from bacteria present in the stained aliquot. In addition, the use of an imaging lens rather than a microscope objective for sample interrogation allows larger depths-of-field and the fluorescence measurement is not constrained to a thin volume on the surface as in microscopy. Therefore, the reported mean fluorescent signal reported by the system provides a better assessment of the number of bacteria present in the culture aliquot. Since the permeable SYBR Green dye binds very reliably to DNA material in each bacteria with high efficiency (> 99% of individual bacteria labelled) [25], we consider that the fluorescence signal averaged over the large field-of-view of the cytometer reader is directly proportional to the number of bacteria present. This indicates that, similarly to the optical density measurement, the available models for bacterial growth apply to our situation. In addition, in order to compare optical density and fluorescence measurements we generate, we will transform the signal collected as $I(t) = \ln(C(t)/C_0)$. C is the intensity of the signal averaged over the entire CMOS image sensor at incubation time t and C_0 is the signal averaged of the CMOS sensor before any sample is introduced and is analogous to the incident light power used for optical density measurements. $I(t)$ constitutes a direct measurement and does not require complex image post-processing. Figure 3(B) shows the typical growth curve obtained and the fit to the logistic population growth model [24]. The fit was obtained in two steps to avoid biasing the algorithm. First, the low and high asymptotes (A_R and B_R constants in Eq. (2)) were determined by holding the seed ratio, x_0, and the maximum growth rate, r, equal to the values determined for the reference optical density curve (Fig. 3(A)) since the aliquots tested came from the same culture sample and we wished to compare the benchmarked method to the reference method for which the models given in Eqs. (1) and (2) were originally developed. The goal of this approach is not to determine experimental growth parameters since the samples tested originate from the same culture. However, this allows to compare the values obtained for each method and evaluate our cytometer approach to a universally-recognized method that may also have some weaknesses to describe the actual complex situation of bacterial growth. Once the data was normalized, A_R and B_R were held to 1 and 0, respectively, while the other parameters were adjusted to minimize the residual error (χ^2) and determine the apparent values for the growth curve measured by the cytometer using Eq. (2). We obtained $x_0 = 0.017 \pm 0.005$ and $r = 0.0120 \pm 0.0009$ s^{-1} with $\chi^2 = 4.77\ 10^{-3}$. These values are still in good agreement with the reference parameters obtained in Fig. 2(A). The actual value of x_0 obtained in Fig. 2(B) suffer from a large imprecision because of the lack of sensitivity for lower bacterial concentrations. In addition, different growth preparations performed on different days can be quite different due to the dormant state in which some bacteria can be in when seeded. Therefore, the actual experimental error on the seed fraction x_0 is much higher than the mathematical error given by the fitting algorithm since it refers to the number of cells introduced that will actually replicate and not necessarily the number of total cells introduced. The data in Fig. 3(B) was obtained by averaging the signal over the 3 consecutive measurements of each triplicate data point by systematically removing the highest and lowest values. Data points at low concentrations were power fluctuations may also influence the quality of the signal were ignored in the fit and omitted from Fig. 3(B). For comparison purposes, the first reliable data point for the growth curve

Biomedical Optics EXPRESS

obtained by the cytometer was offset to overlap with the optical density curve. The error bars represent ± 2σ where σ is the standard deviation. The fit to the Gompertz-Zwietering model yielded k_Z = 0.0031 ± 0.0007 s^{-1} and T_{lag} = 165 ± 4 min with χ^2 = 5.43 10^{-4}. Unlike Fig. 3(A), the Gompertz-Zwietering model fits slightly better to the cytometer reader data. This is understandable in this case because the model defines T_{lag} to always occur at 6.6% of the upper asymptote, which is more fitting for the cytometer data since there is a higher incertitude on data points just above the LOD. The lag phase is slightly shorter than for the optical density measurement and is likely due to the lack of sensitivity of the reader for low signal when only a few bacteria are present. The onset of the exponential growth phase and its duration before reaching the stationary phase are, however, well in line with those obtained by absorbance measurements, which gives a good argument towards the relevance of the measurement using our device. The stationary phase plateau is slightly more pronounced than for the absorbance curve, which could originate from signal saturation on the CMOS sensor.

3.4 Improved depth of field compared to classical microscopy

One of the most interesting feature of the surface cytometer is the large field-of-view. This was illustrated with the 1951 USAF test target. Equally important is the large depth-of-field compared to a confocal or epifluorescence microscope. To clarify this property, we measured the signal for a sample of bacteria cultured in the exponential phase while moving the surface plane of the cytometer to several positions using a precision 1/2" translation stage (Thorlabs CT1) and moving the focal plane of the microscope using the piezoelectric-driven objective positioner. Rather than measuring the actual depth-of-field of the system (about 3 mm using the 1951 USAF target), we chose the more practical information obtained by comparing the distribution of the signal from fluorescently-labelled *E. coli* normal to the surface between the surface cytometer and the confocal microscope. To add to the relevance of this distribution for the accuracy of counting bacteria on a surface, we also characterized the evolution of this distribution upon addition of common fixatives, such as ethanol and glutaraldehyde. These are known chemicals used in microscopy to fix bacteria for surface imaging [33].

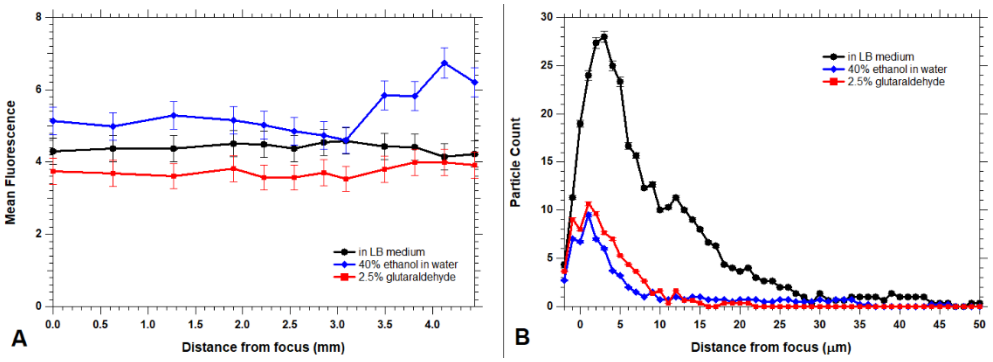

Fig. 5. Evolution with the distance from the surface (focus) of (A) the mean fluorescence in the green channel of the surface cytometer device compared to (B) the fluorescent particles counted for confocal images in the Z-stack for an *E. coli* culture sample in the exponential phase (OD = 2.0). The sample was stained with SYBR Green directly in the LB culture medium (black circles, ●), after fixation with glutaraldehyde at 2.5% (v/v) final (red squares, ■), or absolute ethanol to 40% (v/v) final (blue diamonds, ♦). The higher depth-of-focus results in a much higher measurement volume in the surface cytometer compared to traditional microscopy.

Figure 5(A) shows the evolution of the mean fluorescence obtained on the green channel of the surface cytometer sensor with the distance from the focused image of the surface. As expected, the signal remains almost identical over more than 3 mm. The evolution of the fluorescence signal with the distance from the surface differs only slightly with or without

Biomedical Optics EXPRESS

glutaraldehyde added to the LB medium at 2.5% (v/v) final after staining with SYBR Green. This suggests a very low fixation efficiency at this concentration of glutaraldehyde. However, the addition of 40% (v/v) absolute ethanol to the medium after staining produces a much sharper change in the signal indicating that most bacteria are closer to the surface when fixed with ethanol. The increase in signal rather than a decrease outside of the depth-of-field seems counterintuitive, but we attributed it to the background signal from defocused objects since we simply consider the mean of pixel intensity in the central region of the CMOS-ISA.

For comparison, the same measurement series was performed on the confocal microscope. Figure 5(B) shows the result from particle counting in the 53 frames acquired in series as a Z-stack between a distance of 2 µm below the surface and 50 µm above the surface. The evolution trend for each measurement series (averaged from 3 to 4 stacks) is similar to that in Fig. 5(A). However, the effect of glutaraldehyde is more pronounced because, most likely, of the higher vertical resolution (1 µm stack separation). More importantly, all curves show an abrupt drop in particles counted from the fluorescence images after only 10 µm. This is more than 2 orders of magnitude smaller than for the surface cytometer and illustrates the improvement in the depth-of-field and the ability of the surface cytometer to average the signal over a larger volume and experience less bias from the bacteria distribution from the surface to the bulk of the sample.

3.5 Comparison to other methods used to study bacterial biofilm formation

Some of the most important parameters for the different existing methods to monitor bacteria film formation are the limit of detection (LOD) and the measurement time. Table 1 compares the proposed surface cytometer to other recognized techniques using some of the essential criteria for point-of-care biofilm measurements. Our device offers a similar LOD than existing systems with the clear advantage of fast measurement times, which enables real-time detection, and portability while using simple commercial microscope glass slides rather than complex custom sensor surfaces.

Table 1. Comparison of our method to other available ones for bacterial biofilm monitoring.

Method	LOD		Time (min)	Real-time	Portability	Substrate	Reference
	cells/mL	cells/mm^2					
This work	-	10^4	< 1	Yes	Yes	Glass	-
FISH	10^4	-	< 5	Yes	Yes	Glass	[19]
qPCR	-	10^2	> 60	No	No	Custom	[11]
UV	-	10^4	< 1	Yes	No	UV-grade	[15]
Colorimetric	10^2	-	> 60	No	Yes	Custom	[17]
Magnetic	-	10^3	< 1	Yes	Yes*	Direct	[5]
SERS	10^2	10^4	< 20	No	No	Custom	[9]
Electrochemical	10^2	-	> 20	No	No	Custom	[8]

* requires a network analyzer to read the response.

4. Conclusions

Through the study of bacterial growth curves and the benchmarking against two routinely used methods to generate bacterial growth curves, we have validated a CMOS-based fluorescence reader, named surface cytometer, for an accurate and reliable determination of bacterial growth assessment in a culture aliquot using model Gram-negative bacteria (*E. coli*). We have shown the ability to generate bacterial growth curves that show the same trend as the ones obtained by a gold-standard scattering method. With respect to other imaging techniques, such as fluorescence microscopy, the proposed device has several clear

Biomedical Optics EXPRESS

advantages, including a higher field-of-view and depth-of-field, which place it in an ideal position to measure bacteria biofilms on surfaces with minimal sample preparation in only a few minutes. In addition, our measurement method provides a direct result without the need for complex post-processing. In our approach, the overall time-to-result is between 15 and 20 min, which illustrates the advantage of our system for a rapid count of the total bacteria in a sample at the expense of specificity. The use of more specific antibody-coupled detection probes or labelled nucleic acids would improve the specificity of the detection, but also significantly affect the time-to-result due to the added sample preparations steps.

Appendix: Supplementary information

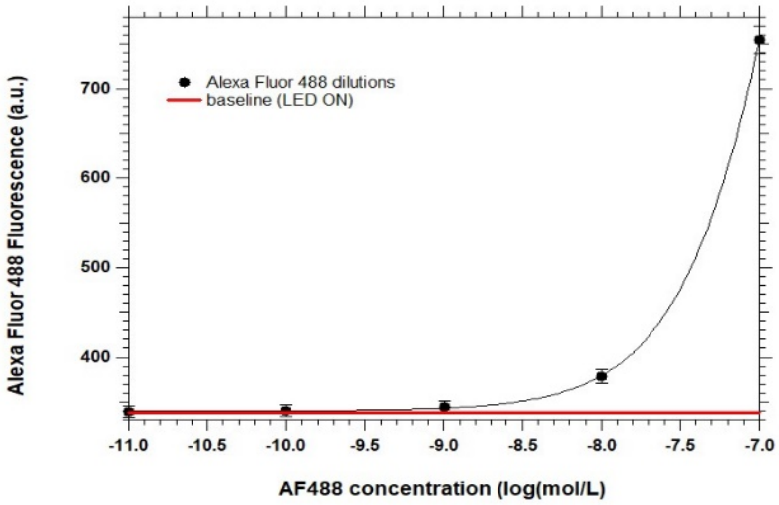

Fig. 6. Evolution of the fluorescence signal detected by the CMOS-ISA sensor for a serial dilution of Alexa Fluor 488 (AF488) dye in deionized water. The red curve represents the average baseline value for deionized water when the LED is ON. The first data point above the baseline occurs for 1-2 nM of AF488, which determines the practical limit of detection (LOD) of the system for a diluted molecular fluorescent dye.

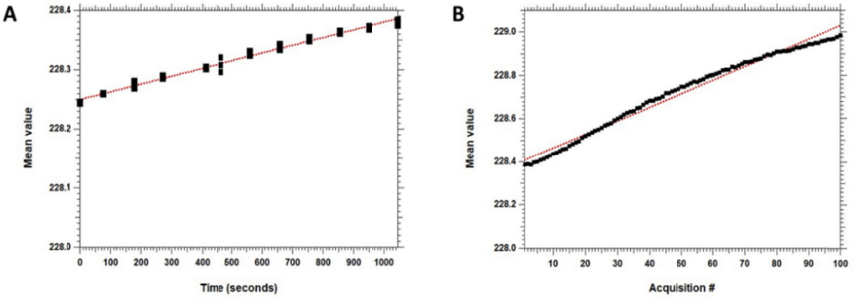

Fig. 7. Stability of the LED used in the surface cytometer setup (color and interference excitation filters removed). (A) Evolution of the signal acquired by the CMOS-ISA in the same experimental conditions as the ones used to monitor bacterial growth (3 100-ms captures separated by 5 s over a total time of 17 minutes. (B) Evolution of the signal acquired by the CMOS-ISA for 100 consecutive captures (exposition: 100 ms) separated by 5 s. In both cases, the drift of the LED (50% duty cycle and 20 MHz) was only 0.26% over more than 17 minutes. This is negligible compared to the changes in the signal from bacterial growth. The red line is a linear fit to appreciate the drift.

Biomedical Optics EXPRESS

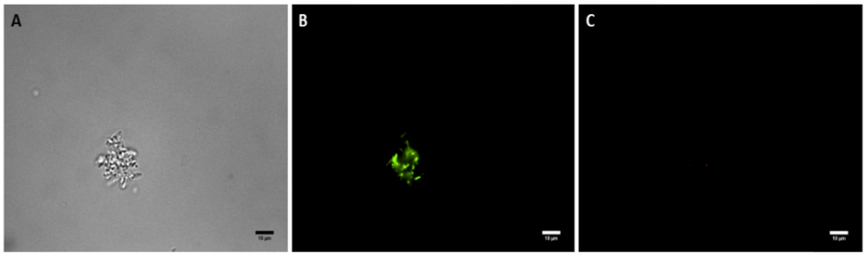

Fig. 8. Transmission microscope image (A) of a fresh culture aliquot stained first with SYBR Green I for 20 min, then with Propidium Iodide for 5 min. All bacteria present on the surface appeared green from the SYBR nucleic acid stain in the green (FITC) channel (B) of the Nikon Ti-U epifluorescence microscope, but no red signal appeared in the red (excitation CWL = 488 nm/emission CWL = 600 nm) channel (C). This indicates the validity of our assumption that a vast majority of the samples obtained immediately from a fresh culture are alive.

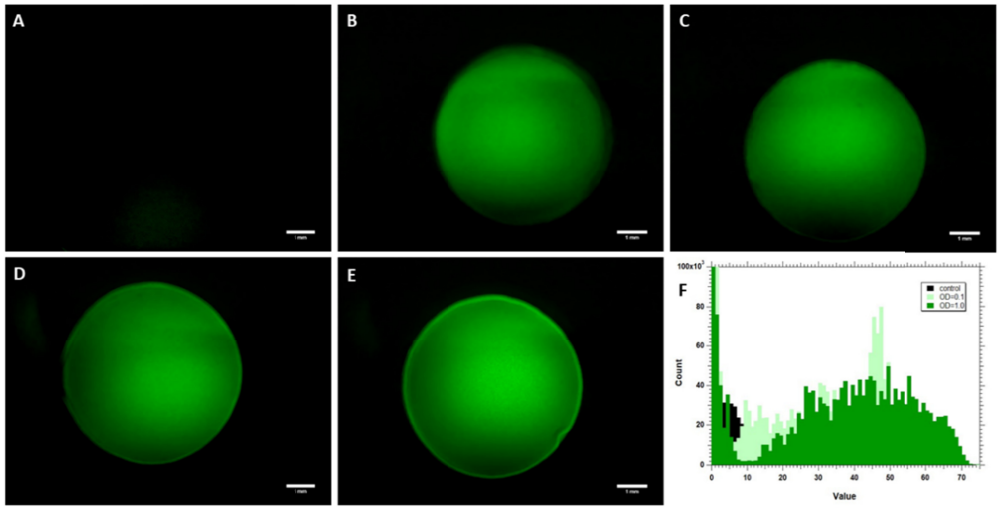

Fig. 9. Images form the CMOS-ISA of the surface cytometer for a control made of only PBS buffer (A), a bacterial culture sample stained with SYBR Green I at an OD value of 0.1 (B), 0.25 (C), 0.5 (D), and 1.0 (E). The red, green, and blue channels were split and the shown green channel was subtracted with the average of the blue and red channel to take the camera response into account. (F) is the evolution of the histogram count for the control and the samples at OD = 0.1 and OD = 1.0 and illustrates the evolution of the green signal.

Funding

Spanish Ministry of Economy and Competitiveness through the Severo Ochoa Programme for Centres of Excellence in R&D (SEV-2015-0522) and OPTO-SCREEN (TEC2016-75080-R), from Fundacio Privada Cellex, from Generalitat de Catalunya through the CERCA program and AGAUR 2017 SGR 1634.

Acknowledgments

The authors acknowledge the help of César Alonso and Dr. Ángel Sandoval from the Bio Lab Research Technical Support at ICFO for help with bacterial culture and useful discussions.

Disclosures

The authors declare that there are no conflicts of interest related to this article.

Biomedical Optics EXPRESS

References

1. J. Azeredo, N. F. Azevedo, R. Briandet, N. Cerca, T. Coenye, A. R. Costa, M. Desvaux, G. Di Bonaventura, M. Hébraud, Z. Jaglic, M. Kačániová, S. Knøchel, A. Lourenço, F. Mergulhão, R. L. Meyer, G. Nychas, M. Simões, O. Tresse, and C. Sternberg, "Critical review on biofilm methods," Crit. Rev. Microbiol. **43**(3), 313–351 (2017).
2. H. C. Flemming, J. Wingender, U. Szewzyk, P. Steinberg, S. A. Rice, and S. Kjelleberg, "Biofilms: an emergent form of bacterial life," Nat. Rev. Microbiol. **14**(9), 563–575 (2016).
3. H. L. Røder, S. J. Sørensen, and M. Burmølle, "Studying Bacterial Multispecies Biofilms: Where to Start?" Trends Microbiol. **24**(6), 503–513 (2016).
4. *PatientCareLink*, Massachusetts Health & Hospital Association, Inc. (2018). *https://patientcarelink.org/improving-patient-care/healthcare-acquired-infections-hais/*
5. Y. Chai, S. Horikawa, S. Li, H. C. Wikle, and B. A. Chin, "A surface-scanning coil detector for real-time, in-situ detection of bacteria on fresh food surfaces," Biosens. Bioelectron. **50**, 311–317 (2013).
6. Y. Lu, S. Horikawa, I. H. Chen, S. Du, H. C. Wikle, S. J. Suh, and B. A. Chin, "Highly sensitive surface-scanning detector for the direct bacterial detection using magnetoelastic (ME) biosensors," Proc. SPIE **10217**, 1021703 (2017).
7. S. Horikawa, I. H. Chen, S. Du, Y. Liu, H. C. Wikle, S. J. Suh, J. M. Barbaree, and B. A. Chin, "Method for Detection of a Few Pathogenic Bacteria and Determination of Live versus Dead Cells," Proc. SPIE **9864**, 98640H (2016).
8. X. Liu, M. Marrakchi, D. Xu, H. Dong, and S. Andreescu, "Biosensors based on modularly designed synthetic peptides for recognition, detection and live/dead differentiation of pathogenic bacteria," Biosens. Bioelectron. **80**, 9–16 (2016).
9. H. Wang, Y. Zhou, X. Jiang, B. Sun, Y. Zhu, H. Wang, Y. Su, and Y. He, "Simultaneous Capture, Detection, and Inactivation of Bacteria As Enabled by a Surface-Enhanced Raman Scattering Multifunctional Chip," Angew. Chem. Int. Ed. Engl. **54**(17), 5132–5136 (2015).
10. H. Zhou, D. Yang, N. P. Ivleva, N. E. Mircescu, R. Niessner, and C. Haisch, "SERS Detection of Bacteria in Water by in Situ Coating with Ag Nanoparticles," Anal. Chem. **86**(3), 1525–1533 (2014).
11. M. P. Buttner, P. Cruz-Perez, and L. D. Stetzenbach, "Enhanced Detection of Surface-Associated Bacteria in Indoor Environments by Quantitative PCR," Appl. Environ. Microbiol. **67**(6), 2564–2570 (2001).
12. Z. A. Islamy Mazrad, I. In, K. D. Lee, and S. Y. Park, "Rapid fluorometric bacteria detection assay and photothermal effect by fluorescent polymer of coated surfaces and aqueous state," Biosens. Bioelectron. **89**(Pt 2), 1026–1033 (2017).
13. X. W. Hua, Y. W. Bao, H. Y. Wang, Z. Chen, and F. G. Wu, "Bacteria-derived fluorescent carbon dots for microbial live/dead differentiation," Nanoscale **9**(6), 2150–2161 (2017).
14. H. Schmidt and T. Eickhorst, "Detection and quantification of native microbial populations on soil-grown rice roots by catalyzed reporter deposition-fluorescence *in situ* hybridization," FEMS Microbiol. Ecol. **87**(2), 390–402 (2014).
15. L. R. Dartnell, T. A. Roberts, G. Moore, J. M. Ward, and J. P. Muller, "Fluorescence Characterization of Clinically-Important Bacteria," PLoS One **8**(9), e75270 (2013).
16. S. M. Yoo and S. Y. Lee, "Optical Biosensors for the Detection of Pathogenic Microorganisms," Trends Biotechnol. **34**(1), 7–25 (2016).
17. M. Safavieh, M. U. Ahmed, E. Sokullu, A. Ng, L. Braescu, and M. Zourob, "A Simple Cassette as Point-of-Care Diagnostic Device for Naked-eye Colorimetric Bacteria Detection," Analyst (Lond.) **139**(2), 482–487 (2014).
18. J. M. Pérez, M. Jofre, P. Martínez, M. A. Yáñez, V. Catalan, and V. Pruneri, "An image cytometer based on angular spatial frequency processing and its validation for rapid detection and quantification of waterborne microorganisms," Analyst (Lond.) **140**(22), 7734–7741 (2015).
19. V. Müller, J. M. Sousa, H. C. Koydemir, M. Veli, D. Tseng, L. Cerqueira, A. Ozcan, N. F. Azevedo, and F. Westerlund, "Identification of a pathogenic bacteria in complex samples using a smartphone based fluorescence microscope," RSC Advances **8**(64), 36493–36502 (2018).
20. M. Berney, F. Hammes, F. Bosshard, H. U. Weilenmann, and T. Egli, "Assessment and interpretation of bacterial viability by using the LIVE/DEAD BacLight kit in combination with flow cytometry," Appl. Environ. Microbiol., **73**, 3283–3290 (2007).
21. P. Stiefel, S. Schmidt-Emrich, K. Maniura-Weber, and Q. Ren, "Critical aspects of using bacterial cell viability assays with the fluorophores SYTO9 and propidium iodide," BMC Microbiol. **15**, 36 (2015).
22. M. H. Zwietering, I. Jongenburger, F. M. Rombouts, and K. van't Riet, "Modeling of the Bacterial Growth Curve," Appl. Environ. Microbiol. **56**(6), 1875–1881 (1990).
23. K. M. C. Tjørve and E. Tjørve, "The use of Gompertz models in growth analyses, and new Gompertz-model approach: An addition to the Unified-Richards family," PLoS One **12**(6), e0178691 (2017).
24. H. Fujikawa and S. Morozumi, "Modeling Surface Growth of Escherichia coli on Agar Plates," Appl. Environ. Microbiol. **71**(12), 7920–7926 (2005).
25. H. Zipper, H. Brunner, J. Bernhagen, and F. Vitzthum, "Investigations on DNA intercalation and surface binding by SYBR Green I, its structure determination and methodological implications," Nucleic Acids Res. **32**(12), e103 (2004).
26. P. Soille and L. M. Vincent, "Watersheds in Digital Spaces: An Efficient Algorithm Based on Immersion Simulations," Proc. SPIE **1360**, 240–250 (1990).

Biomedical Optics EXPRESS

27. A. C. Yu, J. F. Loo, S. Yu, S. K. Kong, and T. F. Chan, "Monitoring bacterial growth using tunable resistive pulse sensing with a pore-based technique," Appl. Microbiol. Biotechnol. **98**(2), 855–862 (2014).
28. H. E. Kubitschek, "Cell Volume Increase in *Escherichia coli* after Shifts to Richer Media," J. Bacteriol. **172**(1), 94–101 (1990).
29. J. Schindelin, I. Arganda-Carreras, E. Frise, V. Kaynig, M. Longair, T. Pietzsch, S. Preibisch, C. Rueden, S. Saalfeld, B. Schmid, J. Y. Tinevez, D. J. White, V. Hartenstein, K. Eliceiri, P. Tomancak, and A. Cardona, "Fiji: an open-source platform for biological-image analysis," Nat. Methods **9**(7), 676–682 (2012).
30. H. H. Tuson and D. B. Weibel, "Bacteria-surface interactions," Soft Matter **9**(17), 4368–4380 (2013).
31. Y. Chao and T. Zhang, "Optimization of fixation methods for observation of bacterial cell morphology and surface ultrastructures by atomic force microscopy," Appl. Microbiol. Biotechnol. **92**(2), 381–392 (2011).
32. A. I. Dragan, R. Pavlovic, J. B. McGivney, J. R. Casas-Finet, E. S. Bishop, R. J. Strouse, M. A. Schenerman, and C. D. Geddes, "SYBR Green I: fluorescence properties and interaction with DNA," J. Fluoresc. **22**(4), 1189–1199 (2012).
33. A. K. Kniggendorf, T. W. Gaul, and M. Meinhardt-Wollweber, "Effects of Ethanol, Formaldehyde, and Gentle Heat Fixation in Confocal Resonance Raman Microscopy of Purple Nonsulfur Bacteria," Microsc. Res. Tech. **74**(2), 177–183 (2011).